

Mechanical properties of amorphous silicon carbonitride thin films at elevated temperatures

Radim Ctvrtlik · Marwan S. Al-Haik ·
Valeriy Kulikovskiy

Received: 26 August 2014 / Accepted: 8 November 2014 / Published online: 21 November 2014
© Springer Science+Business Media New York 2014

Abstract The mechanical properties of amorphous silicon carbonitride ($a\text{-SiC}_x\text{N}_y$) films with various nitrogen content ($y = 0\text{--}40$ at.%) were investigated in situ at elevated temperatures up to 650 °C in inert atmosphere. A SiC film was measured also at 700 °C in air. The hardness and elastic modulus were evaluated using instrumented nanoindentation with thermally stable cubic boron nitride Berkovich indenter. Both the sample and the indenter were separately heated during the experiments to temperatures of 300, 500, and 650 °C. Short duration high temperature creep tests (1200 s) of the films were also carried out. The results revealed that the room temperature hardness and elastic modulus deteriorate with the increase of the nitrogen content. Furthermore, the hardness of both the a-SiC and the a-SiCN films with lower nitrogen content at 300 °C drops to approx. 77 % of the corresponding room temperature values, while it reduces to 69 % for the a-SiCN film with 40 at.% of nitrogen. Further increase of temperature is accompanied with minor reduction in hardness except for the a-SiCN film with

highest nitrogen content, where the hardness decreases at a much faster rate. Upon heating up to 500 °C, the elastic modulus of the a-SiCN film decreases, while it increases at 650 °C due to the pronounced effect of short-range ordering. The steady-state creep rate increases at elevated temperatures and the a-SiC exhibits slower creep rates compared to the a-SiCN films. The value of the universal constant $x = 7$ relating the W_p/W_t and H/E^* was established and its applicability was demonstrated. Analysis of the experimental indentation data suggests a theoretical limit of hardness to elastic modulus ratio of 0.143.

Introduction

The ability to measure the nano- and micro-mechanical properties and microstructure of thin films under elevated temperatures (i.e., at relevant service temperatures) is vital for both the basic scientific investigation and the practical applications. Since materials are usually exposed to elevated temperatures during the manufacturing or application, the room temperature measurements are inadequate as portion of the deformation is thermally activated. For example, at high temperature applications the hardness and yield stress of a material typically decrease leading to thermal softening and excessive wear.

Materials for high temperature applications have to meet a variety of specific physical and chemical properties such as high melting point, appropriate elasticity and acceptable remaining high-temperature strength, creep resistivity together with compositional and structural stability, and acceptable oxidation and corrosion rates. Low density is also desirable in transportation and aerospace applications.

Amorphous silicon carbonitride ($a\text{-SiC}_x\text{N}_y$) thin films can provide all of these, and many additional, outstanding

R. Ctvrtlik (✉)
RCPTM, Joint Laboratory of Optics, Palacky University,
17. listopadu 12, 771 46 Olomouc, Czech Republic
e-mail: ctvrtlik@fzu.cz

M. S. Al-Haik
Department of Biomedical Engineering and Mechanics, Virginia
Tech, Blacksburg, VA 24061, USA

V. Kulikovskiy
Institute of Physics, Academy of Sciences of the Czech
Republic, Na Slovance 2, 182 21 Prague 8, Czech Republic

V. Kulikovskiy
Institute for Problems of Materials Science, Academy of
Sciences of Ukraine, 3 Krzhyzhanovsky St., Kiev 03142,
Ukraine

properties due to the formation of a strongly bonded three-dimensional structural network. Depending on the molar composition they can exhibit extremely high hardness [1], elevated-temperature creep resistance [2], oxidation resistance at temperatures up to 1600 °C [3], low friction coefficient [4], attractive tribological properties [5], tunable optical properties [6, 7], and multitude of other desirable properties. Therefore, a-SiC_xN_y coatings are considered for high temperature wear protective applications due to their excellent thermal and mechanical properties. In addition, their chemical inertness and the possibility to tailor their electrical conductivity make them attractive for micro-electromechanical systems (MEMS) [8–10] and sensor applications like heat flux sensors, sensors for turbines and power generation systems and high temperature/pressure transducers [11, 12]. Amorphous silicon carbonitride is also a promising material for microporous ceramic membranes for high-temperature separation of hydrogen [13]. Furthermore, there is a growing interest in SiC and N-doped SiC as prospective materials capable of replacing silicon in harsh environment applications, such as high temperatures and nuclear radiation [14]. For example, SiC was investigated as a potential replacement of zirconium-based alloys used as cladding for nuclear fuel in water-cooled reactors [15, 16].

Despite the eminent importance of exploring the evolution of the mechanical properties of thin films and coatings at elevated temperatures (hardness and elastic modulus, size effects and deformation mechanisms), few studies can be cited [17–20]. The investigation of the mechanical properties at elevated temperatures has been stymied by the lack of appropriate instrumentation with sufficient resolution and stability as well as the lack of experimental standards and protocols. However, with the recent advances in instrumentation, nanoindentation at elevated temperatures has become more common and reliable. A brief overview of high temperature instrumented indentation studies can be found in [21], including creep experiments [22–24], hardness and modulus evaluation [25], or studies of discrete events occurring beneath the indenter at elevated temperature [26]. More recently, nanoindentation at elevated temperatures has also been proven to be capable of exploring the negative stiffness [27] behavior of certain materials. Nevertheless, performing in situ nanoindentation experiments at elevated temperatures is still hindered by several technical and experimental issues such as thermal and electronic drift of the instrument, effect of isothermal contact (heating of indenter and sample) [28], sample and indenter oxidation (specially for diamond-based indenters) [29] as well as the validity of room temperature routines and calibrations to high temperature tests.

The room temperature hardness for different forms of SiC has been examined thoroughly for both thin films and

coatings [30, 31] and bulk materials, whereas the information on high temperature mechanical properties is limited to sintered ceramics [32–34] or single crystal [35, 36]. Similarly, the published mechanical properties of SiC_xN_y films are exclusively obtained under room temperature conditions either for as-deposited or annealed films [30, 37, 38]. While the high temperature hardness and elastic modulus data for SiC_xN_y films are highly sought for improving their performance these data are not yet available.

In this study, the localized mechanical properties of various a-SiC_xN_y thin films (hardness (H), effective elastic modulus (E^*), H/E^* ratio, and indentation elastic and plastic works) were determined from the nanoindentation testing performed under Ar atmosphere within temperature range of 25–650 °C.

Experimental details

Thin films

Amorphous SiC_xN_y films with thicknesses of 2.9–3.5 μm were deposited on unheated 0.5 mm thick Si(111) substrates by reactive direct current magnetron sputtering. The SiC_x hot-pressed powder target (75 mm in diameter) containing small excess of carbon (for electrical conductivity) was sputtered in the gas mixture of argon and nitrogen at various (N₂/Ar) gas flow ratios of 0, 0.04, 0.16, and 0.48 using the Leybold-Heraeus Z 550 M sputtering system.

The system was evacuated to a base pressure of $\sim 5 \times 10^{-4}$ Pa. The target-substrate distance was 50 mm, and the discharge power was 340 W. The (N₂/Ar) flow ratio was changed from 0 to 0.48 by varying the N₂ flow rate (0, 1, 4, and 12 sccm) while maintaining the Ar flow rate at 25 sccm using mass flow meters. The total pressure varied in the range of 0.5–0.6 Pa. A bias voltage of about -70 V was applied to the substrate holder using a 13.56 MHz power source. The substrate bias and other deposition conditions were chosen based on preliminary experiments with hard and dense amorphous SiC films [31].

Analytical methods

The structure of the deposited films was investigated using Raman spectroscopy. The spectra were measured in the backscattering configuration using the JY Horiba LabRam HR800 unit equipped with 514.5 nm argon laser. The polarization of scattered light was not analyzed. The spectra were measured in the range 200–2000 cm⁻¹, to cover the interval where also the peaks corresponding to various carbon–nitrogen vibrations are expected.

The composition of the as-deposited films was determined by the electron probe X-ray microanalysis using

JEOL JXA-733 electron probe with Kevex Delta Class V microanalyzer. The films thicknesses were measured by an ALFA-STEP profilometer. The surface of each film was examined with an optical microscope and environmental scanning electron microscope (ESEM, FEI Quanta 600 FEG) equipped with an energy-dispersive spectrometer for chemical analysis.

The nanoindentation experiments were carried out using a fully calibrated NanoTest instrument from Micro Materials, Inc. (Wrexham, UK) with a boron nitride Berkovich indenter in load controlled mode at room and elevated temperatures up to 650 °C under Ar and 700 °C in air.

The NanoTest is equipped with a hot stage module which allows reliable measurements at temperatures as high as 750 °C [23]. This feature is possible due to the fact that indentation is performed horizontally and thus allowing the installation of a thermal shield. The heating element has localized effects so that minimal heat flow and thermal drift occurs during indentation at high temperatures. As shown in Fig. 1, an aluminum thin shield is placed in front of the pendulum to prevent any thermal interference with the electronics. The indenter and its heater pass through the thermal shield. The sample is mounted on a ceramic plate

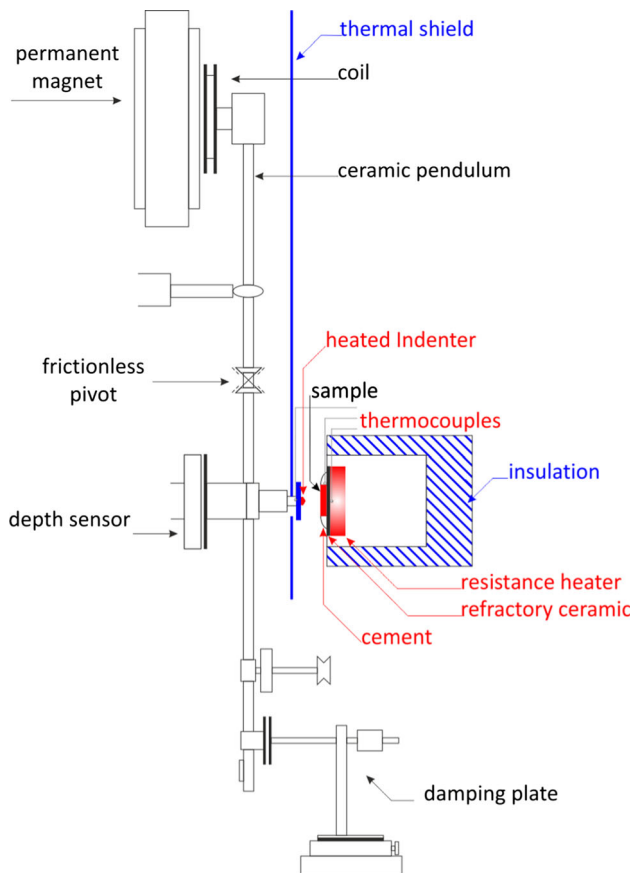


Fig. 1 Schematic of the NanoTest hot stage setup

and the sample heater is embedded inside a thermally insulated block.

A cubic boron nitride (c-BN) indenter, instead of diamond one, was utilized throughout this study. This choice was made to avoid the likely oxidation of diamond beyond 400 °C and its chemical reaction with the samples at elevated temperatures [39]. All the tests were carried out under argon-rich environment to minimize both the sample and indenter oxidation. Samples with lateral dimensions of 5 mm × 5 mm were mounted, using a thin layer of high temperature cement, on the refractory ceramic hot block. The specimen temperature was monitored and controlled via two thermocouples; one mounted beneath the sample and the other on the sample's surface. During the high temperature experiments an autonomous heating control system was utilized for the indenter to minimize heat transfer between the sample and indenter ensuring iso-thermal contact [28].

An indentation maximum load of 12.5 mN was utilized to ensure that the indentation depths remain below 10 % of the film thickness, to avoid the substrate effect, and hence, the calculated hardness and modulus values can be considered film-dominated properties even at elevated temperatures. Both the loading and unloading rates were set to 0.625 mN/s and the dwell period at maximum load was set to 10 s. At least ten indentations were performed at each temperature.

Besides nanoindentation, nanocreeep experiments with prolonged dwell period of 1200 s at peak load of 30 mN were carried out. Samples were annealed at each test temperature for approx. 5.5 h. After cooling down, nanoindentation measurements were repeated at room temperature to evaluate the post-annealing mechanical properties.

The most crucial issue of measurements at elevated temperatures is the thermal drift. In order to improve the stability of the sample/indenter contact, the indenter was held in contact with the sample surface for 120 s prior to starting the indentation. The thermal drift of the system was monitored during the 60 and 90 s lasting period at 90 % unloading for indentation and creep experiments, respectively. The thermal drift correction was calculated from this data and applied during the raw data analysis.

Standard analysis was used to determine the hardness and reduced elastic modulus (E_r) from at least 10 independent indentations curves [40]. The reduced indentation modulus E_r that takes into account also the elastic deformation of the indenter is defined as

$$\frac{1}{E_r} = \frac{1 - \nu^2}{E} + \frac{1 - \nu_i^2}{E_i}, \quad (1)$$

where E and ν , and $E_i = 879$ GPa and $\nu_i = 0.12$, describe the room temperature Young's modulus and Poisson's ratio of the sample and the c-BN indenter, respectively [41, 42].

The effective modulus E^* (also referred to as the elastic modulus) characterizes the sample properties only and is calculated as

$$E^* = \frac{E}{1 - \nu^2}. \quad (2)$$

The effective modulus is calculated after quantifying the c-BN indenter contribution in Eq. (1) and will be considered in this study. It should be noted that the effective modulus is the only valid parameter to correctly compare elastic moduli obtained with different indenters.

Additional short time annealing experiments were also performed in order to discuss the effect of time exposure at elevated temperatures. As-deposited samples were annealed at 700 °C for 30 min under Ar.

Results

Composition

The thickness and composition of the as-deposited films are summarized in Table 1. The variation in the films thicknesses stems primarily from the different sputtering rate that increases with the increase of the (N_2/Ar) ratio [30]. The tested films possess different nitrogen contents ranging from 0 to 40 at.%, with corresponding Si/C ratios increasing from 0.85 to 1.00. The oxygen content in the films is consistent and is less than 2 at.% and is not indicated in the table. The films compositions depend only on the implemented deposition conditions since the amorphous nature did not force the growing film to develop a specific stoichiometry. It should be noted that SiCN does not have a nature analog; there is no single crystal of SiCN in nature.

Mechanical properties

Representative nanoindentation load–displacement hysteresis for a-SiC and a-SiCN film deposited at $N_2/Ar = 0.48$ at different testing temperatures are plotted in Fig. 2. The figures indicate an increase in the indentation depth and

also greater plasticity (greater area between the loading and unloading curves) as a result of increasing the test temperature. Both effects are more pronounced for the a-SiCN film compared to the a-SiC film. The hardness and elastic modulus results for all the nanoindentation tests at peak load of 12.5 mN are summarized in Fig. 3.

Since the elastic properties of the c-BN indenter change with temperature, it was necessary to use an appropriate value of its elastic modulus in Eq. (1) in order to accurately extract the sample properties at particular temperature [41, 42]. Poisson's ratio for the c-BN also changes with temperature, however the amount of this change and its effect on indentation results were found to be almost negligible and within the deviation of the measurement [39]. A 50 % change in indenter Poisson's ratio results in less than 1 % change in elastic modulus in this work. Therefore, the Poisson's ratio for the c-BN indenter was assumed to be constant over the range of temperatures reported.

The data in Table 1 and Fig. 3 clearly show that the hardness and elastic modulus of the as-deposited a-SiC_xN_y films reduce with the increase of nitrogen concentration. The hardness declines from 21.7 GPa for a-SiC_{1.17} film to 18.9 GPa for the film with 40 at.% of nitrogen, while the elastic modulus decreases from approx. 295–241 GPa.

Nanoindentation experiments performed at 300 °C revealed a pronounced decrease in hardness to approx. 77 % of the corresponding room temperature value for the a-SiC and the a-SiC_xN_y films comprising up to 27 at.% of nitrogen. Further increase of nitrogen concentration to 40 at.% is accompanied with a slightly higher drop in hardness from 18.9 to 13.1 GPa corresponding to 69 % of the room temperature value. The elastic modulus measured at 300 °C trails identical trend like the hardness and its values reach approx. 90 % of corresponding room temperature values for each film.

Increasing the temperature from 300 to 500 °C yielded further decrease of both the hardness and the elastic modulus. Ramping the temperature to 650 °C leads to further minor reduction in hardness. However, unlike the hardness, the elastic modulus gradually decreases when the temperature increases up to 500 °C. Further heating up to 650 °C leads to increasing the modulus to values that are comparable to those obtained at room temperature; probably due to gradual improvement of the short-range order taking place beyond 500 °C. The hardness of the a-SiC film drops at an identical rate for the 6H-polytype SiC single crystal up to 300 °C [35]. At higher temperatures the single crystal hardness decreases monotonously at the same rate, while for the a-SiC film hardness reduction rate declines. It should be noted that the softening rate of SiC single crystal was reported considerably lower than for other refractory materials like TiC, W₂C, TiB₂, ZrB₂, Al₂O₃ [35, 43, 44].

Only the a-SiCN film with the highest nitrogen content exhibits more pronounced drop in hardness down to 10 GPa at

Table 1 Thickness and composition of the investigated a-SiC_xN_y thin films

N_2/Ar (–)	Thickness (μm)	Composition		
		Si (at.%)	C (at.%)	N (at.%)
0	2.9	46	54	0
0.04	3.2	41	46	14
0.16	3.3	35	38	27
0.48	3.5	30	30	40

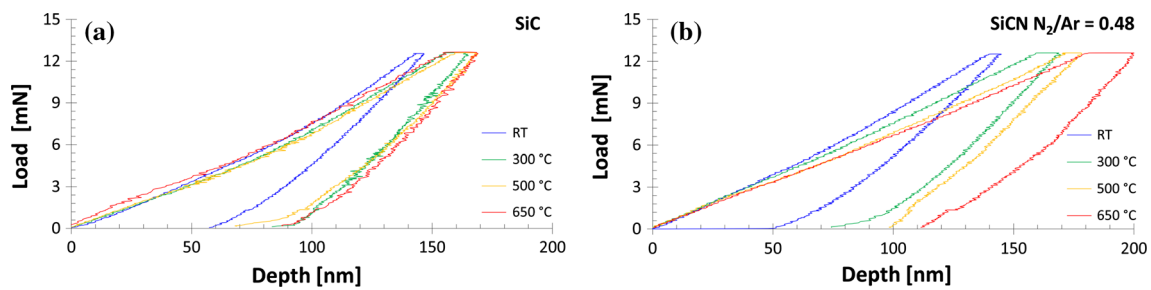


Fig. 2 Representative load–displacement curves for **a** a-SiC and **b** a-SiCN films measured in situ at different temperatures up to 650 °C

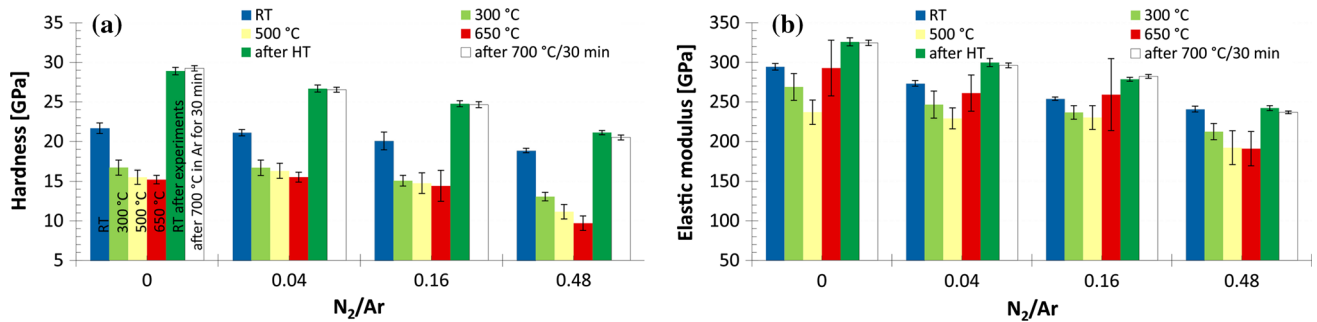


Fig. 3 Mechanical properties of a-SiC_xN_y thin films measured at various temperatures up to 650 °C (samples were exposed at each temperature for approx. 5.5 h); **a** hardness and **b** elastic modulus.

Room temperature data for the post-annealed films after the high temperature experiments (RT after experiments) and the Ar annealing for 30 min at 700 °C are added for comparison

650 °C. The elastic modulus of this film remains practically identical to that measured at 500 °C. The stronger softening for this particular film, deposited at the N₂/Ar = 0.48, can be attributed to the presence of triple bonds between N and C atoms observed in IR transmission spectra [30]. This strong C≡N bond terminates one possible bond with nitrogen as it prevents its further networking with the surrounding atoms. Consequently, development of a strong 3D random network is hindered and the ability of the material to support load and hence hardness are reduced.

Results of nanoindentation tests performed on post-annealed samples; after high temperature experiments, are also shown in Fig. 3. One can notice a significant rise in hardness for all the investigated films; this can be attributed to the improvement of interatomic bonds in the films during high temperature exposure. The extent of this increase reduces with increasing the nitrogen content. The hardness of the post-annealed a-SiC was found to be 33 % higher than that for the as-deposited film, while for the a-SiCN film comprising the maximum N₂/Ar ratio, the post-annealing hardness was only 12 % higher than the as-deposited value. In general, the elastic moduli of the post-annealed films are ~10 % higher than the as-deposited ones except for the film with the highest nitrogen content. For this particular a-SiCN film, the post-annealing elastic modulus was found to be identical to that for the as-deposited film. The enhancement of the mechanical

properties in the binary Si–C system can be attributed to the much easier organization in SiC clusters in comparison to the ternary Si–C–N system where the N atoms hinders the diffusion of Si and C atoms. It is well known that the hardness and modulus of sputtered a-SiC film increase after annealing due to the short-range ordering followed by partial crystallization at higher temperatures [31].

In order to discuss the effect of the annealing duration associated with the utilized experimental setup the films were also annealed at 700 °C for 30 min in Ar. Both the hardness and elastic modulus values after 30 min annealing are almost identical to those post high temperature indentation experiments lasting approx. 5.5 h at each temperature. Air annealing at the same conditions gives very similar values of mechanical properties [30]. This suggests that the processes leading to the atomic short-range ordering are relatively fast and are concluded during 30 min under the implemented experimental conditions. This leads to the conclusion that longer treatment at temperatures around 675 °C does not promote, at least noticeable, further structural ordering of a-SiC_xN_y thin films.

Raman spectra

The degree of structure ordering of the films pre and post the high temperature experiments was investigated using the micro-Raman spectroscopy. In particular, this

scattering technique is suitable for identifying carbon polymorphs and carries the advantage of high special resolution of approx. 1 μm . Raman spectra of all the as-deposited films and films after high temperature nanoindentation experiments are shown in Fig. 4. Since all the spectra were measured under the same conditions; their intensities can be compared directly as there is no offset of the curves in the figures.

The typical Raman spectrum for SiC film exhibits broad bands around 500 cm^{-1} (Si–Si bonds), below 800 cm^{-1} (Si–C bonds), and above 1400 cm^{-1} (C–C bonds) as shown in Fig. 4a. The band around 245 cm^{-1} can be ascribed to the Si–C vibration in the acoustic phonon region. The presence of these bands manifests the coexistence of C-rich and Si-rich amorphous domains together with clusters of amorphous SiC in these films [31]. It should be noted that the film deposited at $N_2/Ar = 0$ possesses a small excess of

carbon ($\text{Si}_{0.47}\text{C}_{0.53}$). The higher intensity of carbon band in comparison to Si–Si and Si–C is a result of the higher Raman polarizability of the C–C bond [45].

The introduction of nitrogen to the SiC film results inevitably in the creation of C–N and Si–N bonds. Particularly, Si–N bonds are chemically more favorable due to the higher difference in their electronegativities. The increasing nitrogen content in the films leads to the rise of the overall intensity of scattered light that corresponds to the decrease of extinction coefficient (ellipsometrical data are not presented). This effect is especially strong for the carbon band that also slightly shifts to higher frequencies with growth of nitrogen concentration due to the increasing presence of C–N bonds, see Fig. 4b. No traces of C=N (about 1600 cm^{-1}) and $\text{C}\equiv\text{N}$ (about 2000 cm^{-1}) related vibration modes were observed in the Raman spectra in lieu to those present in the IR spectra [30]. The absence of these multiple bonds indicates the good interatomic linking that is reflected in the high values of mechanical properties. The intensities of a-SiN_x features in Raman spectra are generally weak as can be seen from the weak bands centered at about 400 and 1000 cm^{-1} [46], especially for the film with the highest nitrogen content. The Si–C related features are very weak or vanished as supported by the IR spectrum [30]. The band about 700 cm^{-1} is considered as a weak feature of pure a-C characteristic especially for sputtered films [47, 48]. Its intensity is considerably enhanced in the presence of nitrogen [49].

Figure 4c shows the Raman spectra of the films post the high temperature nanoindentation experiments performed up to 650 °C in Ar. The general character of the spectra remains identical to the as-deposited samples. There is a considerable increase in scattering intensity due to the increase of scattering volume yielding from the improvement of atomic bonding and decrease of the absorption of the incident laser beam. Moreover, some characteristic bands are enhanced around 450, 700, and 1000 cm^{-1} . There is also noticeable upshift of the carbon G-band and gradual broadening especially for the films with higher nitrogen content. In the case of the film with the highest nitrogen content the low-frequency shoulder on the carbon band indicates the onset of its splitting. Our previous work suggests that this spectrum resembles the one for a film annealed at 900 °C in vacuum for 1 h [30]. No traces of crystalline phase were observed in the post-annealed films.

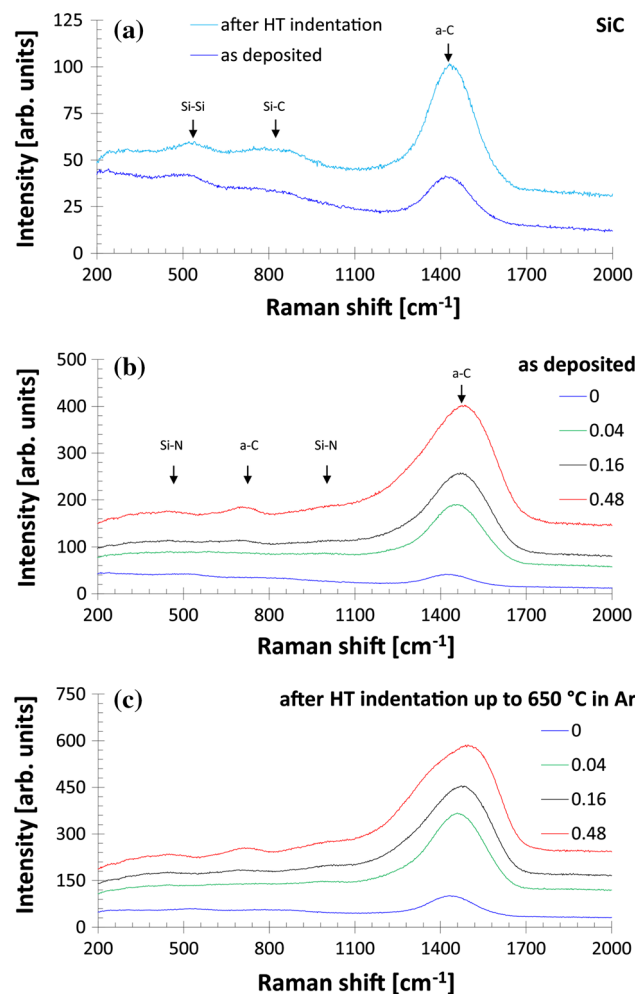


Fig. 4 Raman spectra of the **a** a-SiC films before and after high temperature experiments, and a-SiC_xN_y thin films **b** as-deposited at various N_2/Ar ratios (0–0.48) and **c** after high temperature nanoindentation experiments up to 650 °C in Ar

Discussion

Experimental parameters influence

Our previous study [30] revealed the pronounced effects of annealing the films under atmospheric air on the mechanical properties. In particular, we observed the susceptibility

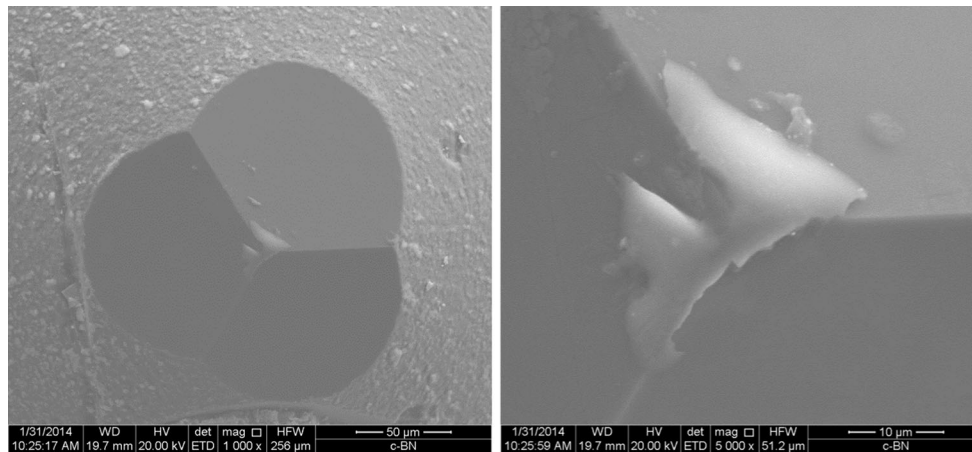


Fig. 5 SEM images of the c-BN Berkovich indenter after experiment at 700 °C in air with developed oxide layer

of $a\text{-SiC}_x\text{N}_y$ films to oxidation under atmospheric air at temperatures above 700 °C and, hence, the current nanoindentation experiments were carried out in inert Ar atmosphere. To delineate the effect of the testing environment, the a-SiC film was also investigated in air up to 700 °C. The post-experiment inspection of the c-BN indenter revealed a heavy contamination on its very tip after conducting a nanoindentation test at 700 °C under atmospheric environment. Figure 5 shows a SEM image of the tip with visible adhered contamination. The energy-dispersive X-ray spectroscopy (EDS) analysis of the contamination (not presented here) revealed strong silicon and oxygen peaks; indicating the formation of SiO_x . This could be linked to the chemical reactivity between the c-BN tip and SiC film under atmospheric air. The tip contamination was not observed for the experiments carried out under Ar environment. As a precaution, the indenter was inspected, cleaned if necessary, and calibrated after each measurement cycle performed on each film sample.

The hardness and elastic modulus values of the a-SiC film measured at 300 °C under air and Ar are almost identical suggesting no or negligible effect of oxidation. At higher temperatures the effect of the Ar and air environments becomes more apparent, especially at shallow indentation depths due to formation of the oxide layer under air environment. This difference reduces with the increase of indentation depth. The formation of relatively soft SiO_x surface layer decreases the rate of further oxidation but does not provide any mechanical support for the underlying layers. On the hardness scale, SiO_x is much softer than Al, Ti, and Cr oxides that are usually employed as tribolayers on the surface of cutting tools [50].

Generally speaking, there are two possible approaches to how to carry out hot stage indentations at various temperatures, namely: one sample can be tested at all temperatures or individual sample tested at each specific temperature. Both approaches possess advantages and disadvantages. In the first

approach only one sample is needed. On the other hand, extended annealing, which might change the microstructure, can occur specially for long-duration experiments. Consequently, the measured mechanical properties can be influenced by the extended heat treating history. Long lasting experiments are also more vulnerable to surface oxidation when tests are performed in atmospheric air environment. This becomes crucial especially at shallow indentation depths. In principle, the one sample per temperature approach can partially surpass the structural changes. But one should bear in mind that the heating and stabilizing procedures prior to the indentation could take several hours and, therefore, both the structural changes and oxidation will still occur.

In this work, one sample was heated and measured stepwise at RT, 300, 500, and 650 °C, while the heating rate was set to 2 °C/min using the NanoTest system thermal controls. It took roughly 5 h to reach and stabilize the nanoindenter/sample temperatures at 300 and 500 °C and 6 h to reach a stable thermal contact at 650 °C. To justify our approach we compared the post-annealed values of the hardness and elastic modulus with those obtained after 30 min annealing at 700 °C in Ar. Figure 3 clearly shows that these values are almost identical. Moreover, our previous work suggests that annealing in air environment at the same experimental condition leads to the same values of hardness and reduced modulus [30]. From this direct comparison it can be concluded that the structural short-range ordering proceeds relatively rapidly during the earliest stages of annealing. The fact that there is no difference in mechanical properties upon 30 min or 360 min annealing duration suggests that the studied $a\text{-SiC}_x\text{N}_y$ films can be considered structurally and mechanically stable at temperatures below 700 °C.

Creep

We limited the creep testing to the samples with most distinctive results; a-SiC and a-SiCN sample with the

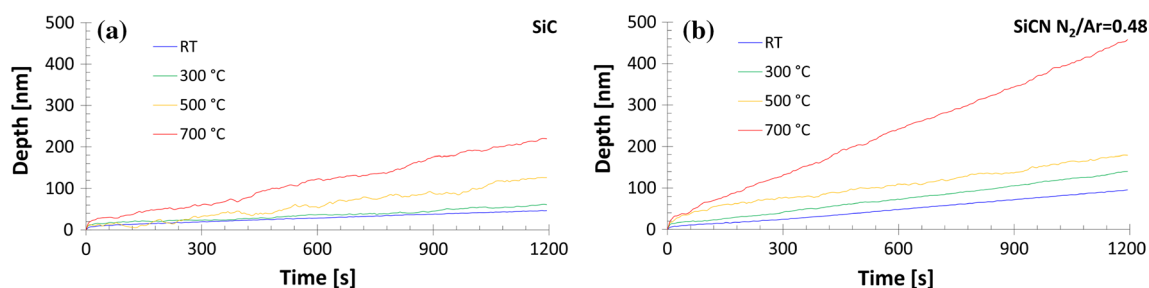


Fig. 6 Creep curves for **a** SiC and **b** SiCN ($N_2/Ar = 0.48$) films measured at constant load of 30 mN for 1200 s at room temperature (RT), 300, 500, and 650 °C

highest nitrogen content ($N_2/Ar = 0.48$). The isothermal creep curves for these films measured at different temperatures up to 650 °C are shown in Fig. 6. The secondary steady-state creep dominates all the creep curves for both samples at all temperatures. The creep rate increases for both samples with the measurement temperature, while it is always smaller for the a-SiC than the a-SiCN film. This is very pronounced at 650 °C where secondary creep rate for the a-SiC is half of that for the a-SiCN film. Literature data for bulk SiC at higher temperatures also show the higher creep resistivity for crystalline SiC than for Si(B)CN materials [51].

In order to quantify the tendency of the films to deform under the constant load indentation the parameter P introduced by Goodall and Clyne was used [52]. It is defined as the product of the slope of the steady-state part of the creep curve, in our case 60–1200 s, and the increase in depth at the end of the constant load period. The higher P value the higher the deformation is expected to occur during the constant load creep. The calculated values of parameter P are presented in Table 2. It can be clearly seen that it monotonously increases with the experiment temperature, while it is lower for a-SiC than a-SiCN.

Indentation work and hardness/elastic modulus ratio

Besides the hardness (H) and the effective elastic modulus (E^*), the ratio H/E^* and plasticity index (defined later) are equally useful and should be evaluated from the high temperature nanoindentation data [53–55]. The H/E^* ratio has been proven to be a more reliable parameter for controlling the wear of the material in lieu of the hardness alone and has been of considerable interest in tribology [56]. Moreover, the H/E^* ratio is related to the elastic strain to failure and appears in many fracture toughness equations [57, 58]. It should be noted that not only high hardness but also sufficient level of toughness are of particular importance in several engineering applications [59, 60]. The importance of toughness and plasticity of the material increases with the severity of the contact [53]. According

Table 2 Calculated values of parameter P quantifying the steady-state creep

Sample	Parameter P (nm^2/s)			
	RT	300 °C	500 °C	650 °C
SiC	1.5	2.3	13.1	38.2
SiCN	7.3	15.0	20.6	163.7

to Zhang et al. [60], the plasticity of a material can be used as a rough indication of how tough the material is.

The plasticity index (W_p/W_t) is defined as a ratio of irreversible plastic work $W_p = W_t - W_e$ to total work W_t done during indentation, where elastic work W_e and W_t are defined as the areas under the unloading and the loading curve, respectively. The difference between these two areas, the area enclosed in-between the loading and unloading parts of the load–displacement curve, defines the irreversible plastic work W_p , i.e., work consumed during plastic deformation. Beake et al. [53] showed that there is a correlation between the plasticity index and tool life for hard coatings.

The gradual decrease of the hardness with increasing the temperature (see Fig. 3) is accompanied by simultaneous increase of W_p/W_t (or decrease of H/E^*) as can be seen in Fig. 7. This indicates the increase of material plasticity at higher temperatures and reflects the role of thermally activated deformation mechanism like atomic diffusion within the film. The W_p/W_t ratio at 650 °C reaches ~145 % of its room temperature value regardless of the film composition. On the other hand, the decrease of plasticity below the level of as-deposited films is observed back at room temperature after the annealing due to the improvement of the films' structure; see Raman spectra in Fig. 4b, c.

The resistance of the tested material against plastic deformation at elevated temperatures is governed by two mechanisms acting against each other. During the indentation test the plastic deformation is enabled by the thermally activated diffusion processes leading to softening of

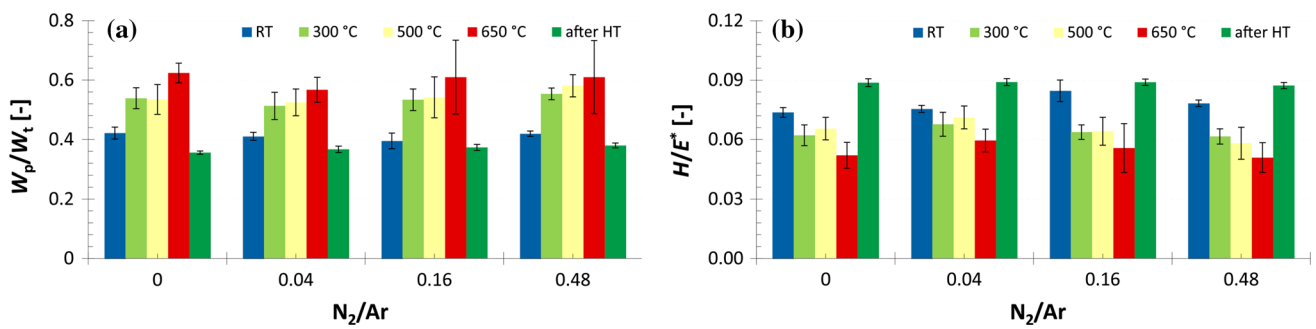


Fig. 7 Plasticity index (W_p/W_t) and H/E^* ratio for the a-Si_xN_y films measured at RT, 300, 500, and 650 °C in Ar

the material. On the other hand, the atomic short-range ordering takes place and cause the improvement of microstructure and, hence, mechanical properties. Which of these two effects prevail depends on the temperature, material structure, and its thermal stability. It should be noted that diffusion also partially promotes microstructural ordering to more thermodynamically stable arrangement. However, during nanoindentation experiment the diffusion is activated by both the high temperature, and high strain and stress gradients beneath the indenter. Moreover, there can also be a different effect on elastic and plastic properties. This can clearly be deduced from Fig. 3, where the hardness gradually decreases up to 650 °C, while the elastic modulus starts to increase above 500 °C. This can be understood in light of the fact that the hardness and elastic modulus are two different characteristics describing different aspect of material behavior [61]. The elastic modulus is an intrinsic material property and its nature is directly related to the atomic bonding. On the other hand, the hardness is associated with plastic deformation mechanics and reflects both the material structure and deformation mechanisms during the test.

Employing finite element modeling (FEM) of elasto-plastic solids with different work hardening, Marx [62] and later Cheng and Cheng in combination with dimensionless analysis [54, 55] formulated a linear relationship between H/E^* and the W_p/W_t ratios over a wide range of H/E^* values

$$\frac{W_p}{W_t} = 1 - x \frac{H}{E^*} \quad (3)$$

The material independent constant $x = 5$ for both Vickers and Berkovich indenter and their representative cone with half-included angle of 70.3° was established predominantly by numerical calculations for the wide range of bulk materials [54, 62–64]. Experimental results reported by Beake et al. [53] proposed that $x = 6–7$ for bulk materials over a wide range of indentation peak forces. The same authors reported an x value around 6.4 for hard coatings. Malzbender and de With also suggested the linear relationship for thin films and coatings [65].

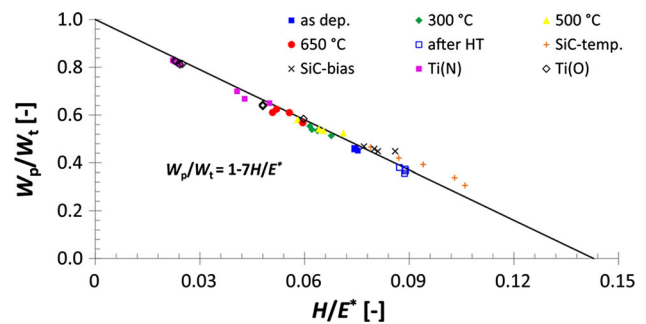


Fig. 8 Universal relationship between W_p/W_t and H/E^* for the a-Si_xN_y thin films measured at temperatures up to 650 °C. SiC films sputtered at various temperatures and biases [31], and N and O doped Ti films [66] are presented to cover wider range of H/E^*

Calculated W_p/W_t versus H/E^* data are shown in Fig. 8. Applying Eq. (3) to our data gives $x = 7$ for all the a-Si_xN_y films regardless of the measurement temperature. This indicates that the linear relationship between W_p/W_t versus H/E^* is applicable even for high temperature nanoindentation measurement of thin films. To support the applicability of $x = 7$ data for various SiC films [31] and N- and O-doped Ti films [66] broadening the range of W_p/W_t and H/E^* are presented. Using Eq. (3) and $x = 7$ for nanocrystalline TiC/amorphous carbon composite films also agrees well with values reported by Voevodin [67]. Since the extreme limits of W_p/W_t are 0 for pure elastic response and 1 for rigid plastic deformation, one can estimate the theoretical limit of H/E^* around 0.143 extrapolating linear relationship (3) provided $x = 7$.

It should be noted that in the case of thin films and coatings the values appearing in Eq. (3) are generally load-dependent. The higher the indentation load the greater the substrate influence especially on the elastic modulus. On the other hand, too low loads can inhibit full plastic development and consequently yield lower hardness. The applicability of Eq. (3) to thin films on substrates is limited only to cases where energy dissipation is not affected by fracture and delamination events [65].

An important implication of the gained knowledge of the interrelationship between W_p/W_t and H/E^* is that the hardness H and reduced modulus E_r can be obtained without the knowledge of the contact area A . Equation (3) together with second independent equation derived from the hardness definition $H = P_{\max}/A$ and equation for initial unloading slope $S = 2E_r(A/\pi)^{1/2}$ in the form of

$$\frac{H}{E^{*2}} = \frac{4P_{\max}}{\pi S^2}, \quad (4)$$

can be solved for H and E_r , using Eq. (1) provided that the initial unloading slope S calculated at maximum load P_{\max} is known. The ratio H/E_r^2 is suggested as the indication of the material's resistance to plastic deformation [68]. The fact that the prior knowledge of the contact area is not necessary for hardness and elastic modulus assessment is beneficial especially for indentations accompanied by material pile-up around the contact impression, where the actual contact area is underestimated by standard Oliver-Pharr procedure [40, 69].

Conclusions

Isothermal nanoindentation tests performed at elevated temperatures up to 650 °C were employed to investigate the stability of mechanical properties of various magnetron sputtered amorphous SiC and SiC_xN_y thin films with nitrogen content up to 40 at.%. One sample, of each configuration, was measured stepwise at all temperatures via c-BN indenter. As the indenter was contaminated with SiO_x after the experiment on a-SiC film in air at 700 °C, all the experiments were carried out in argon environment to prevent samples' oxidation.

The room temperature hardness and elastic modulus decrease with the increase of nitrogen content. All the films show softening at elevated temperatures. Measurements for a-SiC and a-SiCN with the highest nitrogen content at 300 °C revealed a drop in hardness to 77 and 69 % of corresponding room temperature values, respectively. Increasing the test temperature to 500 °C was accompanied by further slight reduction of both hardness and elastic modulus. Unlike the hardness, the elastic modulus gradually decreased by increasing the temperature up to 500 °C; further heating up to 650 °C leads to similar modulus values to those obtained at room temperature. This behavior is likely due to the gradual improvement of short-range order taking place beyond 500 °C.

The comparison of the mechanical properties of the a-SiC_xN_y films after high temperature measurements (300 min at 300 and 500 °C and 360 min at 650 °C) and films annealing at 700 °C for 30 min in Ar constituted the validity of the adopted experimental approach for high

temperature nanoindentation as the values of hardness and elastic modulus are almost identical. This also indicates the good long-time stability of the mechanical properties of a-SiCN at temperatures below 700 °C. The amorphous structure of all the films remains unchanged after annealing during the hot stage experiments; only short-range ordering was observed. No traces of crystalline phase were observed in the post-annealed films.

Gradual decrease of the hardness with increasing the temperature is accompanied by simultaneous increase of the ratio of the plastic to the total indentation works indicating the growth of material plasticity and highlighting the role of thermally activated deformation mechanism like atomic diffusion within the films. The W_p/W_t ratio at 650 °C reaches ~145 % of its room temperature value regardless of the film composition. On the other hand, the decrease of plasticity below the level of the as-deposited films is observed back at room temperature after the annealing due to the improvement of the microstructure.

The value of the universal constant $x = 7$ relating the W_p/W_t and H/E^* was established and its applicability was demonstrated even at elevated temperatures up to 650 °C. Nanoindentation creep tests performed for 1200 s up to 650 °C revealed that a-SiC films possess better creep resistance than the a-SiCN films. The steady-state creep rate increases with the measurement temperature, while it is always smaller for a-SiC than for a-SiCN film.

The results of this study demonstrate the validity and usefulness of high temperature nanoindentation measurements for exploring the thermal stability of the mechanical properties of a-SiCN thin films, as the post-annealing characteristics do not reflect the actual high temperature behavior at the operating high temperatures.

Acknowledgements This work has been supported by the project LO1305 of the Ministry of Education, Youth and Sports of the Czech Republic. Dr. Ctvrtlik also acknowledges the support through the Fulbright Scholar program.

References

1. Badzian A et al (1998) Silicon carbonitride: a rival to cubic boron nitride. *Diam Relat Mater* 7(10):1519–1525
2. An L et al (1998) Newtonian viscosity of amorphous silicon carbonitride at high temperature. *J Am Ceram Soc* 81(5):1349–1352
3. Riedel R et al (1995) A covalent micro nanocomposite resistant to high-temperature oxidation. *Nature* 374(6522):526–528
4. Bielinski D, Wrobel AM, Walkiewicz-Pietrzykowska A (2002) Mechanical and tribological properties of thin remote microwave plasma CVD a-Si:N: C films from a single-source precursor. *Tribol Lett* 13(2):71–76
5. Hoche H et al (2008) Relationship of chemical and structural properties with the tribological behavior of sputtered SiCN films. *Surf Coat Technol* 202(22–23):5567–5571
6. Tomasella E et al (2009) Structural and optical investigations of silicon carbon nitride thin films deposited by magnetron sputtering. *Plasma Processes Polym* 6(SUPPL. 1):S11–S16

7. Sundaram KB, Alizadeh J (2000) Deposition and optical studies of silicon carbide nitride thin films. *Thin Solid Films* 370(1):151–154
8. Liew LA et al (2002) Fabrication of SiCN MEMS by photopolymerization of pre-ceramic polymer. *Sens Actuators A* 95(2–3):120–134
9. Carreño MNP, Lopes AT (2004) Self-sustained bridges of a-SiC: H films obtained by PECVD at low temperatures for MEMS applications. *J Non-Cryst Solids* 338–340(1 SPEC. ISS.):490–495
10. Mehregany M, Zorman CA (1999) SiC MEMS: opportunities and challenges for applications in harsh environments. *Thin Solid Films* 355–356(0):518–524
11. Leo A et al (2010) Characterization of thick and thin film SiCN for pressure sensing at high temperatures. *Sensors* 10(2):1338–1354
12. Yang J (2013) A harsh environment wireless pressure sensing solution utilizing high temperature electronics. *Sensors* 13(3):2719–2734
13. Iwamoto Y (2004) Microporous ceramic membranes for high-temperature separation of hydrogen. *Membrane* 29(5):258–264
14. Wijesundara MJB, Azevedo RG (2011) Silicon carbide microsystems for harsh environments. In: MEMS reference shelf, vol xv. Springer, New York, p 232
15. Lee Y, McKrell TJ, Yue C, Kazimi MS (2013) Safety assessment of SiC cladding oxidation under loss-of-coolant accident conditions in light water reactors. *Nucl Technol* 183(2):8
16. Stempien JD, Carpenter DM, Kohse G, Kazimi MS (2013) Characteristics of composite silicon carbide fuel cladding after irradiation under simulated PWR conditions. *Nucl Technol* 183(1):17
17. Fox-Rabinovich GS et al (2008) Effect of temperature of annealing below 900 C on structure, properties and tool life of an AlTiN coating under various cutting conditions. *Surf Coat Technol* 202(13):2985–2992
18. Lotfian S et al (2012) High-temperature nanoindentation behavior of Al/SiC multilayers. *Philos Mag Lett* 92(8):362–367
19. Lee WS, Liu TY, Chen TH (2009) Nanoindentation behaviour and microstructural evolution of Au/Cr/Si thin films. *Mater Trans* 50(7):1768–1777
20. Beake BD, Fox-Rabinovich GS (2014) Progress in high temperature nanomechanical testing of coatings for optimising their performance in high speed machining. *Surf Coat Tech* 255(0):102–111
21. Schuh CA, Packard CE, Lund AC (2006) Nanoindentation and contact-mode imaging at high temperatures. *J Mater Res* 21(3):725–736
22. Lucas BN, Oliver WC (1999) Indentation power-law creep of high-purity indium. *Metall Mater Trans A* 30(3):601–610
23. Milhans J et al (2011) Mechanical properties of solid oxide fuel cell glass-ceramic seal at high temperatures. *J Power Sour* 196(13):5599–5603
24. Maier V et al (2013) An improved long-term nanoindentation creep testing approach for studying the local deformation processes in nanocrystalline metals at room and elevated temperatures. *J Mater Res* 28(9):1177–1188
25. Beake BD, Smith JF (2002) High-temperature nanoindentation testing of fused silica and other materials. *Philos Mag A* 82(10):2179–2186
26. Schuh CA et al (2005) High temperature nanoindentation for the study of flow defects. Cambridge University Press, Cambridge
27. Skandani AA, Ctvrtlik R, Al-Haik M (2014) Nanocharacterization of the negative stiffness of ferroelectric materials. *Appl Phys Lett* 105(8):082906
28. Everitt NM, Davies MI, Smith JF (2011) High temperature nanoindentation—the importance of isothermal contact. *Philos Mag* 91(7–9):1221–1244
29. Wheeler JM, Oliver RA, Clyne TW (2010) AFM observation of diamond indenters after oxidation at elevated temperatures. *Diam Relat Mater* 19(11):1348–1353
30. Kulikovskiy V et al (2014) Effect of air annealing on mechanical properties and structure of SiC_xN_y magnetron sputtered films. *Surf Coat Technol* 240:76–85
31. Kulikovskiy V et al (2008) Hardness and elastic modulus of amorphous and nanocrystalline SiC and Si films. *Surf Coat Technol* 202(9):1738–1745
32. Atkins AG, Tabor D (1966) Hardness and deformation properties of solids at very high temperatures. *Proc R Soc Lond A* 292(1431):441–459
33. Wachtman JB, Lam DG (1959) Young's modulus of various refractory materials as a function of temperature. *J Am Ceram Soc* 42(5):254–260
34. Kaiser A et al (1997) Hot hardness and creep of Si₃N₄/SiC micro/nano- and nano/nano-composites. *Nanostruct Mater* 8(4):489–497
35. Hirai T, Niihara K (1979) Hot hardness of SiC single crystal. *J Mater Sci* 14(9):2253–2255. doi:10.1007/BF00688433
36. Li Z, Bradt RC (1988) The single crystal elastic constants of hexagonal SiC to 1000 C. *Int J High Technol Ceram* 4(1):1–10
37. Pusch C et al (2011) Influence of the PVD sputtering method on structural characteristics of SiCN-coatings—Comparison of RF, DC and HiPIMS sputtering and target configurations. *Surf Coat Technol* 205(SUPPL. 2):S119–S123
38. Hoche H et al (2010) Properties of SiCN coatings for high temperature applications—comparison of RF-, DC- and HPPMS-sputtering. *Surf Coat Technol* 205(SUPPL. 1):S21–S27
39. Wheeler JM, Michler J (2013) Invited article: indenter materials for high temperature nanoindentation. *Rev Sci Instrum* 84(10):101301
40. Oliver WC, Pharr GM (1992) An improved technique for determining hardness and elastic modulus using load and displacement sensing indentation experiments. *J Mater Res* 7:1564–1583
41. Albe K (1997) Theoretical study of boron nitride modifications at hydrostatic pressures. *Phys Rev B* 55(10):6203–6210
42. D'Evelyn MP, Taniguchi T (1999) Elastic properties of translucent polycrystalline cubic boron nitride as characterized by the dynamic resonance method. *Diam Relat Mater* 8(8–9):1522–1526
43. Farnsworth PL, Coble RL (1966) Deformation behavior of dense polycrystalline SiC. *J Am Ceram Soc* 49(5):264–268
44. Koester RD, Moak DP (1967) Hot Hardness of Selected Borides, Oxides, and Carbides to 1900 C. *J Am Ceram Soc* 50(6):290–296
45. Hillel R et al (1993) Microstructure of chemically vapour codeposited SiCTiCC nanocomposites. *Mater Sci Eng A* 168(2):183–187
46. Wada N et al (1981) Raman and IR absorption spectroscopic studies on α , β , and amorphous Si₃N₄. *J Non-Cryst Solids* 43(1):7–15
47. Basca WS et al (1993) Raman scattering of laser-deposited amorphous carbon. *Phys Rev B* 47:10931–10934
48. Kulikovskiy V et al (2003) Thermal stability of microhardness and internal stress of hard a-C films with predominantly sp² bonds. *Diam Relat Mater* 12(8):1378–1384
49. Vorlíček V et al (1996) C: N and C:N: O films: Preparation and properties. *Diam Relat Mater* 5(3–5):570–574
50. Dosbaeva GK et al (2010) Oxide scales formation in nano-crystalline TiAlCrSiYN PVD coatings at elevated temperature. *Int J Refract Metal Hard Mater* 28(1):133–141
51. Riedel R et al (1998) Amorphous silicoboron carbonitride ceramic with very high viscosity at temperatures above 1500 C. *J Am Ceram Soc* 81(12):3341–3344
52. Goodall R, Clyne TW (2006) A critical appraisal of the extraction of creep parameters from nanoindentation data obtained at room temperature. *Acta Mater* 54(20):5489–5499
53. Beake BD et al (2009) Coating optimisation for high speed machining with advanced nanomechanical test methods. *Surf Coat Technol* 203(13):1919–1925
54. Cheng YT, Cheng CM (1998) Relationships between hardness, elastic modulus, and the work of indentation. *Appl Phys Lett* 73(5):614–616

55. Cheng YT, Cheng CM (2004) Scaling, dimensional analysis, and indentation measurements. *Mater Sci Eng R* 44(4–5):91–150
56. Leyland A, Matthews A (2000) On the significance of the H/E ratio in wear control: a nanocomposite coating approach to optimised tribological behaviour. *Wear* 246(1–2):1–11
57. Lawn BR, Evans AG, Marshall DB (1980) Elastic/plastic indentation damage in ceramics: the median/radial crack system. *J Am Ceram Soc* 63(9–10):574–581
58. Galvan D, Pei YT, De Hosson JTM (2006) Deformation and failure mechanism of nano-composite coatings under nano-indentation. *Surf Coat Technol* 200(24):6718–6726
59. Zhang S et al (2007) Hard yet tough nanocomposite coatings—present status and future trends. *Plasma Processes Polym* 4(3):219–228
60. Zhang S et al (2005) Toughness measurement of thin films: a critical review. *Surf Coat Technol* 198(1–3):74–84
61. Musil J et al (2002) Relationships between hardness, Young's modulus and elastic recovery in hard nanocomposite coatings. *Surf Coat Technol* 154(2–3):304–313
62. Marx V, Balke H (1997) A critical investigation of the unloading behavior of sharp indentation. *Acta Mater* 45(9):3791–3800
63. Giannakopoulos AE, Suresh S (1999) Determination of elastoplastic properties by instrumented sharp indentation. *Scripta Mater* 40(10):1191–1198
64. Choi IC et al (2012) Indentation creep revisited. *J Mater Res* 27(1):3–11
65. Malzbender J, De With G (2000) Energy dissipation, fracture toughness and the indentation load-displacement curve of coated materials. *Surf Coat Technol* 135(1):60–68
66. Firstov S et al (2012) Effect of small concentrations of oxygen and nitrogen on the structure and mechanical properties of sputtered titanium films. *Surf Coat Technol* 206(17):3580–3585
67. Voevodin AA, Prasad SV, Zabinski JS (1997) Nanocrystalline carbide/amorphous carbon composites. *J Appl Phys* 82(2):855–858
68. Joslin DL, Oliver WC (1990) New method for analyzing data from continuous depth-sensing microindentation tests. *J Mater Res* 5(1):123–126
69. Oliver WC, Pharr GM (2004) Measurement of hardness and elastic modulus by instrumented indentation: advances in understanding and refinements to methodology. *J Mater Res* 19(1):3–20